Biomaterials 35 (2014) 6482–6497

Contents lists available at ScienceDirect

Biomaterials

journal homepage: www.elsevier.com/locate/biomaterials

Multifunctional polymersomes for cytosolic delivery of gemcitabine and doxorubicin to cancer cells

Rahul Nahire [a], Manas K. Haldar [a], Shirshendu Paul [d], Avinash H. Ambre [b], Varsha Meghnani [a], Buddhadev Layek [a], Kalpana S. Katti [b], Kara N. Gange [c], Jagdish Singh [a], Kausik Sarkar [d,e], Sanku Mallik [a,*]

[a] Department of Pharmaceutical Sciences, North Dakota State University, Fargo, ND 58108, United States
[b] Civil Engineering, North Dakota State University, Fargo, ND 58108, United States
[c] Health, Nutrition, and Exercise Sciences, North Dakota State University, Fargo, ND 58108, United States
[d] Department of Mechanical Engineering, University of Delaware, Newark, DE 19716, United States
[e] Department of Mechanical and Aerospace Engineering, George Washington University, Washington, DC 20052, United States

ARTICLE INFO

Article history:
Received 7 March 2014
Accepted 8 April 2014
Available online 5 May 2014

Keywords:
Drug delivery
Liposome
Polymersome
Pancreatic cancer
Gemcitabine

ABSTRACT

Although liposomes are widely used as carriers of drugs and imaging agents, they suffer from a lack of stability and the slow release of the encapsulated contents at the targeted site. Polymersomes (vesicles of amphiphilic polymers) are considerably more stable compared to liposomes; however, they also demonstrate a slow release for the encapsulated contents, limiting their efficacy as a drug-delivery tool. As a solution, we prepared and characterized echogenic polymersomes, which are programmed to release the encapsulated drugs rapidly when incubated with cytosolic concentrations of glutathione. These vesicles encapsulated air bubbles inside and efficiently reflected diagnostic-frequency ultrasound. Folate-targeted polymersomes showed an enhanced uptake by breast and pancreatic-cancer cells in a monolayer as well as in three-dimensional spheroid cultures. Polymersomes encapsulated with the anticancer drugs gemcitabine and doxorubicin showed significant cytotoxicity to these cells. With further improvements, these vesicles hold the promise to serve as multifunctional nanocarriers, offering a triggered release as well as diagnostic ultrasound imaging.

1. Introduction

Gemcitabine, a fluorinated nucleoside analog (2′,2′-difluorodeoxycytidine), has emerged as an effective anticancer drug against various malignancies [1] and is currently used in both palliative and adjuvant therapy following surgery for pancreatic cancer. However, the drug is not devoid of limitations. For example, it shows systemic toxicity [2] and has a very short half-life, ranging from 8 to 17 min. In addition, it undergoes rapid conversion to an inactive metabolite in the blood stream [3]. Gemcitabine is a prodrug that requires cellular uptake by the hENT1 receptors on the cancer-cell surface. Unfortunately, a majority of patients (more than 65%) lack this receptor, further limiting the usefulness of the free drug [4].

In order to overcome these limitations, gemcitabine has been delivered by employing various carriers, e.g., theranostic nanoparticles [5], targeted liposomes [6], micelles [7], and microbubbles [8]. Recent clinical studies demonstrate that gemcitabine, in combination with other antineoplastic agents, is more effective for treating pancreatic-cancer [9–13]. For example, due to the non-overlapping toxicity profiles, gemcitabine's efficacy is synergistically enhanced in the presence of the anticancer drug doxorubicin [14–16]. However, this drug combination also has severe side effects [17–19]. Consequently, there is an urgent and unmet need to deliver these drugs to tumor tissues using a drug-delivery vehicle. There is only one report of simultaneous delivery for these two drugs as polymer conjugates [20]. To date, there are no reports about the targeted delivery of this drug combination to pancreatic-cancer cells employing any other drug carrier.

Currently, several liposomal drug formulations are approved by the U.S. Food and Drug Administration to treat cancer. Although these formulations show improved efficacy and safety, most of them still lead to severe side effects [21]. With these formulations, the presence of polyethyleneglycol (PEG) lipids renders the long-circulating property, and facilitates the accumulation of

* Corresponding author.
E-mail address: Sanku.Mallik@ndsu.edu (S. Mallik).

http://dx.doi.org/10.1016/j.biomaterials.2014.04.026
0142-9612/

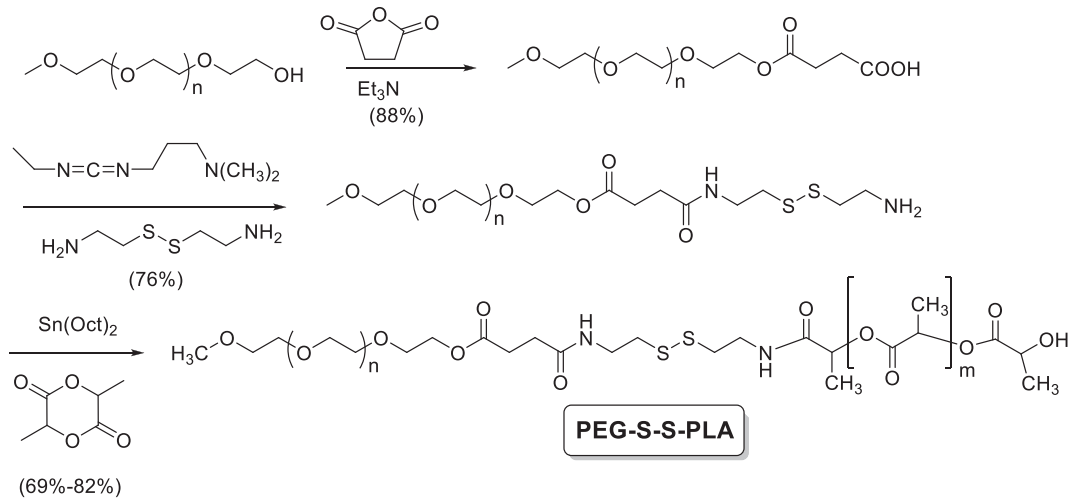

Scheme 1. Synthesis of the diblock disulfide-linked copolymer PEG-S-S-PLA employing the ring-opening polymerization.

liposomes in the tumor tissues due to the enhanced permeation and retention effect [22]. Upon reaching the intended sites, the encapsulated contents are released passively, and this process is often slow [23]. In addition, anti-phospholipid antibodies cause other complications, such as pulmonary hypertension, due to pseudo-allergic reactions [24]. Thus, tunable release, specifically at the target site, would be desirable for a greater therapeutic impact for the drug formulation without compromising its safety profile. Several research groups, including ours, have successfully demonstrated that the integration of targeting and triggering strategies considerably improves the anti-tumor efficacy of liposomal formulations [25,26].

Polymersomes are vesicles prepared from synthetic, amphiphilic-block copolymers [27]. They have several advantages over liposomes, including enhanced stability, longer circulation times, mechanical robustness, and the ability to carry large quantities of hydrophobic and hydrophilic drug molecules [28]. Due to the polymers' higher molecular weights, polymersomes' bilayer membranes are generally thicker, stronger, and hence, inherently more stable than conventional liposomes and micelles. The hydrophilic block of the copolymers is usually polyethyleneglycol, imparting the long-circulating property to the resultant polymersomes [29].

The enhanced stability of the polymersomes also has disadvantages; the release of encapsulated drugs is rather slow [30,31]. Because of robustness, the polymersomes require a stimulus to sufficiently disturb the compact bilayer and to release the encapsulated contents. There are a few reports of targeting [32–36] and content release from polymersomes that employ either internal (pH [37,38], glucose [39], or cysteine [40]) or external triggers (light [41], heat [42], or magnetic field [43]).

In the pursuit of designing stimuli-response polymersomes for simultaneously delivering gemcitabine and doxorubicin to cancer cells, we noted that the concentration of thiol-based reducing agents increases from 10–40 μM in the blood to 1–10 mM in the cell cytosol [44,45]. We are using this differential reducing-agent concentration to cause permanent structural changes in the amphiphilic-block copolymers. We demonstrate that the disturbance created compromises the vesicular structure of the polymersomes, resulting in a rapid release of the encapsulated anticancer drugs. In order to impart multimodal characteristics, we have encapsulated air bubbles as ultrasound contrast agents. In our design, targeting groups (folate-conjugated lipids) on the outside surface of the polymer vesicles ensure the targeting and subsequent facile entry inside the cancer cells. We note that, currently, there are no reports of air-encapsulated, echogenic polymersomes, although the corresponding liposomal counterparts are well documented and characterized [25,26,46].

2. Materials and methods

2.1. Synthesis and characterization of polymers

To synthesize the polymers, first, methoxy-PEG (MW: 1900) was reacted with succinic anhydride in dichloromethane solvent in the presence of triethylamine. The carboxy-terminated PEG thus obtained was subjected to further conjugation with cystamine dihydrochloride in the presence of EDC (ethyl-3-(3-dimethylaminopropyl)-carbodiimide). Finally, polylactic acid (MW: 3600) was prepared by ring-opening polymerization of lactide at the amine terminal of PEG using tin (II) bis(2-ethylhexanoate) as the catalyst under the refluxing condition (Scheme 1) [47]. For the detailed procedure, see the Supporting Information.

2.2. Gel-permeation chromatography

To determine the weight average molecular weights of polymers and disulfide degradation by glutathione, gel-permeation chromatography (Agilent) was performed. THF (tetrahydrofuran) was used to dissolve the polystyrene standards (Supelco) and the polymers. Analysis was done with an Ultrahydrogel 250 (7.8 mm × 300 mm) column with THF as the mobile phase at a flow rate of 0.6 mL/min. Run time was kept at 30 min with refractive-index (RI) detection at room temperature. For each analysis, 50 μL of a sample (1 mg/mL) were injected. The calibration curve for standards was established, and retention times for polymers were extrapolated on the curve to obtain the average molecular weights. To check the sensitivity toward glutathione, the polymers were injected before and after incubation with 5 mM of glutathione for an hour. Changes for the retention times of polymer peaks were noted and compared.

2.3. Differential scanning calorimetry

To determine the melting points of the synthesized polymers, a Nano DSC instrument (TA Instruments) was used. The polymer solution (1 mg/mL) of a 10-mM phosphate buffer (pH 7.0) was used as the sample, and heated from 0 °C to 80 °C at the rate of 1 °C per minute. The phosphate buffer (pH 7.0) was taken as the control. The heating and cooling cycles were repeated twice to ensure reproducibility and reversibility of melting. The collected data were analyzed using Nanoanalyze software (version 4.2.2) provided by the vendor.

2.4. Preparation of polymersomes

2.4.1. Calcein encapsulation

Initially, we prepared polymersomes with the thin-film hydration-sonication and solvent-exchange methods [27]. We observed that the solvent-exchange method produced a narrower-size distribution of polymersomes, and showed higher encapsulation efficiency. Briefly, polymers were dissolved in THF (5 mg/mL) and slowly added to a calcein solution (10 μM) in a 10 mM HEPES buffer (pH 7.4) with constant stirring. After stirring for an hour, THF was removed under a stream of nitrogen gas. The solution was then sonicated for 60 min using a bath sonicator

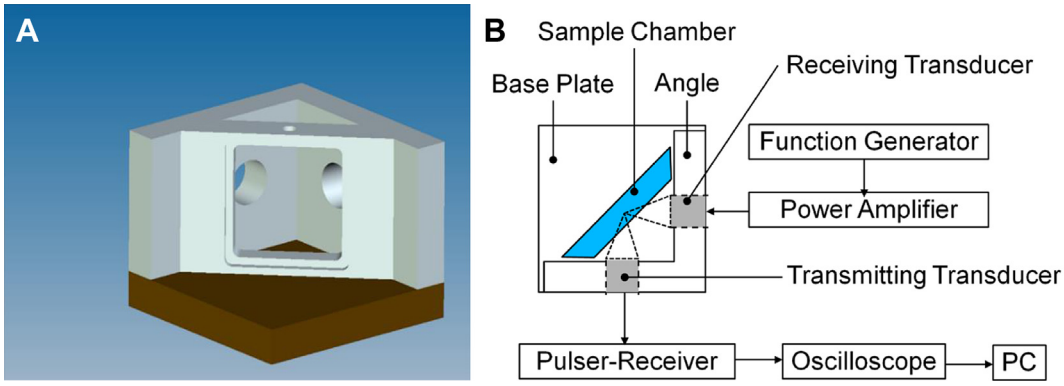

Fig. 1. (**A**) A three-dimensional rendition of the setup used for the acoustic experiments. (**B**) A schematic representation of the setup for in-vitro scattering measurements.

(Aquasonic, Model 250D) at room temperature. The polymersomes were then extruded at 70 °C through polycarbonate membrane filters with a pore size of 1000 nm.

2.4.2. Doxorubicin-gemcitabine encapsulation

Doxorubicin (Bridge Bioservices) and gemcitabine (Matrix Scientific) were encapsulated into the polymersomes with the pH gradient method [48]. The polymersomes were prepared with the solvent-exchange method as described earlier, encapsulating a citrate buffer with a pH of 4.0. Subsequently, the pH of the external buffer was adjusted to 7.0 by adding sodium bicarbonate powder. The polymersomes were then incubated with a mixture (1:1) of gemcitabine and doxorubicin at a 0.2 mg/mL concentration for 3 hours at room temperature. Unencapsulated drugs were removed by passing the polymersomes through a Sephadex™ G-100 (GE Healthcare) size exclusion column. The encapsulation efficiency was established by measuring the absorbance at 276 nm (for gemcitabine) and 480 nm (for doxorubicin) before and after gel filtration.

2.5. Simultaneous determination of doxorubicin and gemcitabine

We used the dual-wavelength UV spectrophotometric method to simultaneously estimate the concentrations of encapsulated doxorubicin and gemcitabine [49]. We selected the two wavelengths as 276 nm and 480 nm. While doxorubicin has the same absorbance at these wavelengths, gemcitabine has negligible absorbance at 480 nm. Thus, gemcitabine can be determined at 276 nm by subtracting the absorbance of doxorubicin at 480 nm, and doxorubicin can be determined at 480 nm (Fig. 11). The method was developed and validated by determining the linear dynamic range and reproducibility.

2.6. Size-distribution analysis

The dynamic light-scattering method (NanoZS 90 Zetasizer, Malvern Instruments) was used to study the polymersomes' size distribution. The polymersomes were dispersed in a 10 mM HEPES buffer (pH 7.4) at a concentration of 0.2 mg/mL in a DTS 0012 polystyrene, disposable sizing cuvette. The measurements were performed at a scattering angle of 90°. The samples were equilibrated for 60 s, and 10 readings were taken for a single sample at a constant temperature (25 °C). Each batch of polymersomes was studied for size distribution, and each experiment was repeated 5 times to check the repeatability of results and to calculate the standard deviation.

2.7. Atomic force microscopy (AFM)

The polymersome samples in a 10 mM HEPES buffer (pH = 7.4) were placed onto a mica sheet and air-dried. To perform AFM imaging, a Multimode™ atomic force microscope with a Nanoscope IIIa controller and J type piezo scanner (Veeco Metrology Group) was used. An antimony (*n*) doped Si-tip was used to obtain images in Tapping Mode™ under laboratory conditions. Images were taken before and after incubation with glutathione (5 mM) for an hour. The effect of the reducing agent on shape and morphology of polymersomes was studied.

2.8. Transmission electron microscopy

The polymersome samples were imaged using a JEOL JEM 2000 transmission electron microscope operating at 100 kV and at low magnifications with the beam spread (not converged) to reduce the amount of electron–beam interaction per unit area and, hence, beam damage to the sample if it were to occur. The polymersome samples in a 10 mM HEPES buffer (pH = 7.4) were dispersed to 1 mg/mL and dropped onto a 300-mesh, Formvar-coated copper grid previously coated with 0.01% poly-L-lysine and allowed to stand for 1 min before wicking off with filter paper. Then, sample was allowed to air dry for 2 min, negatively stained with 1% phosphotungstic acid for 90 s, and subsequently wicked with filter paper and then allowed to dry before being beamed.

2.9. Ultrasound scattering experiment

We studied the echogenic properties of several contrast agents in our earlier publications [25,26,46] utilizing an in-vitro acoustic setup that included a large sample volume (100 mL). Here, we adopted a modified version of that setup with a smaller sample volume (20 mL) to enable experiments at a higher concentration of polymersomes (Fig. 1). The present setup utilized the same confocal arrangement described in our previous publications to have a better signal-to-noise ratio. The setup employed two single-element focused immersion transducers (Olympus NDT, Waltham, MA). A 3.5-MHz and a 5-MHz transducer were used as the transmitter and receiver, respectively. Details about the instrumentation used and data-acquisition procedure can be found in our previous publication [46], and are omitted here for brevity. A 90° angle made of polycarbonate blocks was used for the confocal alignment of the transducers. The drilled holes on each wall of the angle allowed for the insertion of traducers. The angle could be fixed to a base plate that was also made of polycarbonate. An acoustically transparent film (Saran™ wrap) was wrapped around the frame to provide an enclosure for the samples. It forms two acoustically transparent windows. Care was taken to keep the film taut and well stretched to prevent film reflections from corrupting the data in our region of interest. When both the frame (wrapped with the film) and the angle fitted with transducers were affixed to the base plate, the confocal regions of the focused transducer aligned halfway between the acoustically transparent windows. The entire arrangement was placed in a large container with water to keep the sample chamber and the transducers submerged. The water level was adjusted to ensure that it did not spill into the sample chamber.

2.10. Ultrasound imaging

A Terason t3200 diagnostic ultrasound (MediCorp LLC) instrument was used to image the polymersome samples. A layer of Aquasonic 100 (Parker Laboratories) ultrasound gel was applied to a 15L4 linear ultrasound transducer (4–15 MHz; MediCorp, LLC). The gel was placed over parafilm that covered 96 well plates that each contained 200 μL of polymersomes (in 10 mM HEPES buffer, pH = 7.4). The ultrasound scan properties were fixed at 0.7 mechanical index (MI) and 0.6 thermal index (omni Mean activated, level-C image map, level-C persistence, high frequency, level-three TeraVision, level-51 2D gain, level-60 dynamic range, 3-cm scan depth, and 22-Hz frame rate). The Terason diagnostic-imaging instrument measured the reflected ultrasound (not the attenuations) when constructing the images. The images were recorded for polymersomes (0.01 mg/mL) and saved. Images were further analyzed using ImageJ software (version 1.47v, NIH, USA) to calculate the mean and maximum gray scale.

2.11. Triggered-release studies

2.11.1. Redox-triggered release

We used the cobalt quenching method where external, unencapsulated calcein fluorescence is quenched by millimolar concentration of cobalt chloride [50]. The release was monitored using a spectrofluorimeter (Spectramax M5, Molecular Devices) by exciting at 495 nm and recording the emission at 515 nm using a 96-well plate. In each well, 20 μL of the polymersome solution (0.02 mg/mL) was incubated in 10 mM of HEPES buffer (pH 7.4). The release was monitored for 60 min, and measurements were taken at 30-s intervals. Each sample was taken in triplicate, and each study was repeated 3 times to check the repeatability of the results. Release was calculated using the following formula:

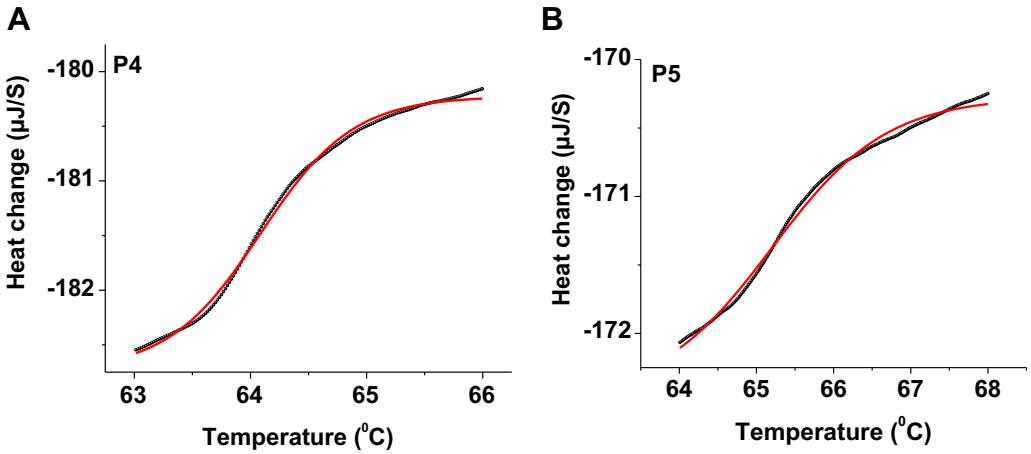

Fig. 2. Differential scanning calorimetric thermograms of polymers (**A**) **PEG_{1900}-S-S-PLA_{5800}** and (**B**) **PEG_{1900}-S-S-PLA_{3600}** (black: observed data points; red: fitted curve). (For interpretation of the references to color in this figure legend, the reader is referred to the web version of this article.)

$$\text{Release}\ (\%) = \frac{\text{Initial intensity} - \text{Observed intensity}}{\text{Initial intensity}} \times 100$$

2.11.2. Ultrasound-triggered release

For the release experiments, a Sonitron 1000® (Richmar) ultrasound instrument was employed. Calcein-encapsulated polymersomes (0.02 mg/mL) were incubated in a 48-well plate with HEPES buffer (10 mM, pH 7.4). The ultrasound-probe tip was immersed into the solution, and ultrasound was applied at different times after incubation for different time intervals. The ultrasound parameters were varied to obtain maximum release from the polymersomes (frequency 1 MHz, 100% duty cycles, 2 W/cm^2, 5 min of application time). The release was monitored on a Spectramax (Molecular Devices) spectrofluorimeter (λ_{ex} = 495 nm, λ_{em} = 515 nm). The percentage release was calculated using the formula mentioned in the previous section. Although the setup used to carry out this study allows reflection of the ultrasound waves from the air–water interface, which gives rise to the standing wave pattern, we note that the setup is adequate to demonstrate the proof of concept. As mentioned in our previous publications, we noticed negligible (less than 1%) energy transfer to adjacent wells during stimulation, indicating almost no inter-well interferences [51,52]. All experiments were performed three times and in triplicate each time to ensure reproducibility of results and to calculate standard deviations.

2.11.3. Simultaneous application of redox and ultrasound triggers

Three different designs were used for these experiments.

(1) Ultrasound (frequency 1 MHz, 100% duty cycles, 2 W/cm^2, 5 min of application time) was applied, followed by a redox trigger (5-mM GSH).
(2) The redox trigger was immediately followed by ultrasound.
(3) The redox trigger was followed by ultrasound after 60 min of incubation.

2.12. Folate-targeting studies

For folate-targeted polymersome uptake studies, PANC-1 (pancreatic ductal carcinoma) and MCF-7 (breast cancer) cells were cultured in clear (without added Phenol red) RPMI media supplemented with 10% fetal bovine serum and 1% antibiotics (penicillin and streptomycin). Both cell lines were purchased from ATCC. The culture flasks were incubated at 37 °C in a humidified atmosphere that contained 5% CO_2. When 90% confluent, the cells were suspended using a trypsin-versene reagent. The suspended cells were then cultured onto sterile, 6-well culture plates until 90% confluent.

Once confluent, the media was removed, and cells were gently washed with HBSS (HyClone®, Thermo Scientific, UT) 5-6 times to completely remove any leftover media. Subsequently, the polymersomes (0.025 mg/mL) were suspended in HBSS and were incubated with the cells for different time intervals. HOESCHT 33342 dye (Enzo Life Sciences, 1 in 1000 dilution) was added to stain the cells' nuclei. After specific time intervals, the polymersome samples were removed from the wells, and the cells were, again, washed with HBSS to remove any polymersomes on the cell surface. Cells were then observed under a fluorescence microscope at different times for uptake. All images were obtained with an Olympus IX81® motorized inverted microscope, viewed using 20× objectives, and captured using CellSens Standard software (version 1.6).

2.13. Cell-viability studies (monolayer culture)

The cytotoxicity of targeted and non-targeted polymersomes was determined by AlamarBlue® assay, measuring the fluorescence of resorufin (red) formed by the reduction of resazurin (blue) in the cytosol of viable cells (metabolically active) [53]. Briefly, PANC-1 and MCF-7 cells were transferred to flat, clear-bottomed, 96-well tissue-culture plates (Corning) at a density of 2×10^4 per well 24 h prior to the assay (or 70–80% confluency). The culture medium in each well was carefully removed and replaced with gemcitabine + doxorubicin encapsulated, folate-conjugated polymersomes; gemcitabine + doxorubicin encapsulated, non-targeted polymersomes; and a free gemcitabine + doxorubicin solution mixed with media. After incubation at 37 °C for 48 h, the cells were washed 3 times with sterile HBSS and incubated in a fresh culture medium. At this point, 20 μL of AlamarBlue® were added to each well, and the fluorescence readings (λ_{ex} = 560 nm, λ_{em} = 590 nm) were taken after 3 h of incubation at 37 °C. Average readings were then compared to the control and plotted.

2.14. Spheroid 3D cell culture studies

The MCF-7 cell spheroids were grown by modifying a published protocol [54]. Briefly, 3% w/v of agar solution were prepared by boiling until it became translucent, to which an equal volume of RPMI media (37 °C) was added. To a 48-well plate, 200 μL of the above mixture were added to each well. Once it solidified, 1×10^5 cells were added to each well and centrifuged at 1000 g for 10 min. The plates were then slowly moved into a humidified incubator without disturbing them and were grown for 3 days. Spheroid growth was monitored for the entire study duration, and then, tests were conducted accordingly.

2.15. Cell-viability studies (spheroid 3D culture)

The spheroids were allowed to grow for 9 days after preparation. On the 10th and 11th days, gemcitabine + doxorubicin loaded polymersomes (targeted and non-targeted), and the free-drug combination were dispersed in media and incubated with the spheroids for 48 h. Control spheroids were incubated with polymersomes without any encapsulated drugs. After treatment for 48 h, the spheroid growth was monitored for 21 days by taking microscopic images.

3. Results and discussion

3.1. Polymer synthesis, polymersome preparation, and structural characterization

The hydrophilic fraction (f) of an amphiphilic-block copolymer determines its ability to form bilayer vesicles. The formation of polymersomes is favored when the ratio of hydrophilic mass to the total mass of the polymer is similar to that of the naturally occurring phospholipids, with an f value of 35% ± 10% [29]. In order to optimize vesicle formation, we synthesized 5 polymers with varying f values from 25% to 68%. We kept the PEG molecular weight constant at 1900, and varied the molecular weights for the PLA (Polylactic acid) portion from 900 to 5800. Thus, we synthesized polymers with an average PLA molecular weight of 900, 1700, 1950, 3600, and 5800 by ring-opening polymerization [55]. To incorporate the disulfide bond, m-PEG (MW 1900) was first reacted with succinic anhydride, followed by conjugation of cystamine. The resulting m-PEG derivative with free amine at one terminal was

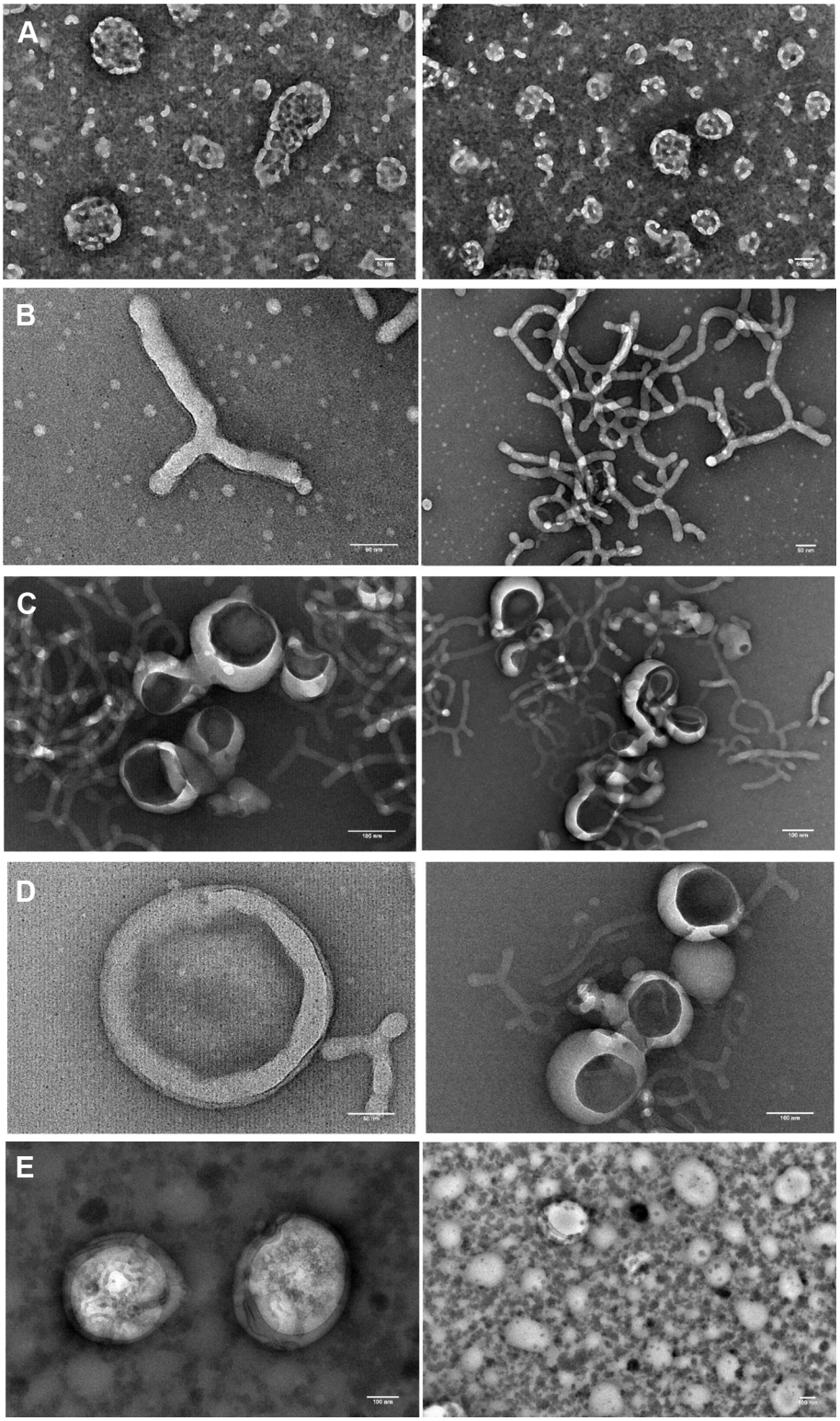

Fig. 3. Transmission electron microscopic images of negatively stained polymersomes: (A) **P1**, (B) **P2**, (C) **P3**, (D) **P4**, and (E) **P5**.

used for all polymer syntheses (Scheme 1). Polymers were purified, and their average molecular weights were confirmed by ^{1}H NMR spectroscopy and gel-permeation chromatography (Supporting Information).

Although several protocols have been reported for preparing polymersomes, the thin-film rehydration and solvent-exchange methods are most common [28]. If the copolymers have a low Tg (glass transition temperature below 25 °C), polymersomes can be prepared by directly putting them into water. In contrast, if the hydrophobic block has a high Tg (above 25 °C), the copolymers do not form polymersomes with such a treatment. In this situation, a suitable organic solvent needs to be used (solvent-exchange

Table 1
Diblock, amphiphilic, redox-sensitive copolymers and their observed morphology.

Polymer	% Hydrophilic fraction	Observed morphology	Polymersome name
PEG_{1900}-S-S-PLA_{900}	68	Micelles, small spheres	–
PEG_{1900}-S-S-PLA_{1700}	53	Mostly bicelles, worms	–
PEG_{1900}-S-S-PLA_{1950}	49	Mostly bicelles, a few vesicles	–
PEG_{1900}-S-S-PLA_{3600}	35	Mostly bilayered vesicles, a few bicelles	**P4**
PEG_{1900}-S-S-PLA_{5800}	25	Bilayered vesicles (polymersomes)	**P5**

method) to lower the Tg of the hydrophobic polymer block. This solvent provides enough chain mobility for the polymers to form the bilayered vesicles [27].

To determine the optimal method to form the polymersomes, we analyzed the thermal properties of the synthesized polymers by using differential scanning calorimetry (DSC). We subjected the polymers in a 10 mM phosphate buffer (pH 7.0) to gradual (1 °C per minute) heating in DSC from 0 °C to 80 °C. We noticed that all the polymers had a transition temperature well above 60 °C (representative thermograms for **PEG_{1900}-S-S-PLA_{3600}** and **PEG_{1900}-S-S-PLA_{5800}** are shown in Fig. 2). We observed that polymers **PEG_{1900}-S-S-PLA_{3600}** and **PEG_{1900}-S-S-PLA_{5800}** had glass transition temperatures of 64.1 °C and 65.2 °C, respectively (Fig. 2). These results suggested that the solvent-exchange method would be most suitable for preparing the polymersomes. Glass transition temperatures well above the body temperature also ensured stability for the polymersomes in circulation with minimal passive leakage and, hence, reduced systemic toxicity.

Having determined the optimal method for preparing polymersomes, we dissolved the polymers in THF and slowly added this solution to an aqueous buffer. Subsequently, N_2 gas was slowly passed over the mixture to evaporate THF. The resultant samples were lyophilized and observed under transmission electron microscopy (Fig. 3).

Due to the presence of the hydrophilic PEG and the hydrophobic PLA domains, PEG-PLA block copolymers spontaneously aggregated into different structures in an aqueous buffer [56]. We also observed that the hydrophilic fraction (f) of the synthesized amphiphilic-block copolymers (Table 1) determined their ability to form different structures, e.g., micelles, bicelles, worms, and vesicles (Fig. 3). When the f value was highest (68% for PEG_{1900}-S-S-PLA_{900}; Table 1), micelles were formed with a size around 50–100 nm (Fig. 3, Panel **A**). PEG_{1900}-S-S-PLA_{1700} (f = 53%) and PEG_{1900}-S-S-PLA_{1950} (f = 49%) polymers only showed bicelles and long, worm-like structures with a few ill-formed vesicles (Fig. 3, Panels **B** and **C**). Well-structured vesicles were only formed from PEG_{1900}-S-S-PLA_{3600} (f = 35%) and PEG_{1900}-S-S-PLA_{5800} (f = 25%) polymers (Fig. 3, Panels **D** and **E**). These results were also corroborated by atomic force microscopy (Fig. 6, before treatment). We also noticed that the bilayer thickness was about 20–30 nm for the **P4** and **P5** polymersomes (Fig. 3, Panels **D** and **E**), which is much larger than liposomes (with a bilayer thickness around 3–5 nm) [56].

Because only the PEG_{1900}-S-S-PLA_{3600} and PEG_{1900}-S-S-PLA_{5800} polymers formed vesicles (polymersomes **P4** and **P5**, respectively, Table 1), all further studies were performed with these two formulations. We determined the average size distributions, zeta potentials, and electrophoretic mobility values of these polymersomes using a dynamic light-scattering instrument (Table 2). We observed that the average hydrodynamic diameter of the **P5** polymersome (209 ± 34 nm) was higher compared to **P4** (157 ± 68 nm). This difference in size is likely due to the higher molecular weight of the PEG_{1900}-S-S-PLA_{5800} polymer compared to PEG_{1900}-S-S-PLA_{3600}. Dynamic light-scattering experiments also showed that the size distribution was quite disperse, ranging from 25 nm to 700 nm (Fig. 4). These sizes for the polymersomes are large and may not be ideal for passive tumor targeting that employs the enhanced permeability and retention effect [57]. However, the vesicles can be extruded to smaller sizes, if needed, for future applications.

3.2. Structural studies in the presence of reducing agents

Prior to any release studies with polymersomes, we tested the copolymers' sensitivity toward reducing agents. In this endeavor, the PEG_{1900}-S-S-PLA_{3600} and PEG_{1900}-S-S-PLA_{5800} copolymers were dissolved in THF and exposed to the reducing agent glutathione (GSH, 5 mM). Because cytosolic-concentration glutathione (GSH) ranges from 5 mM to 15 mM [45], we incubated the copolymers with 5 mM of GSH for an hour and then determined any degradation by gel-permeation chromatography (Fig. 5). The retention times (R_t) of both copolymers (PEG_{1900}-S-S-PLA_{3600} and PEG_{1900}-S-S-PLA_{5800}) showed a shift toward lower average molecular weight (increased R_t) components, indicating cleavage of the disulfide bond that connects the PEG and PLA parts.

We also studied the effect of glutathione (5 mM) on the morphology and size of the **P4** and **P5** polymersomes by employing atomic force microscopy. We observed that, before treatment, the polymersomes were spherical (Fig. 6, before treatment). After 1 h of

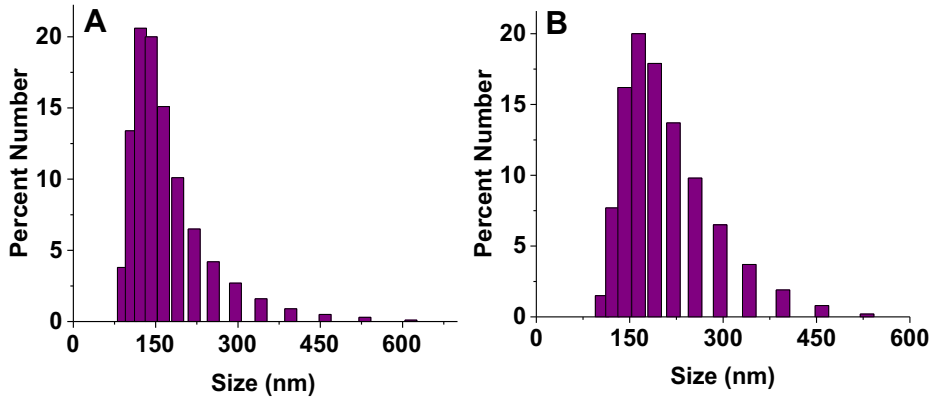

Fig. 4. Representative size distribution for the number of structures formed by different polymers with the dynamic light-scattering method using a Zetasizer instrument: (A) **P4** and (B) **P5**.

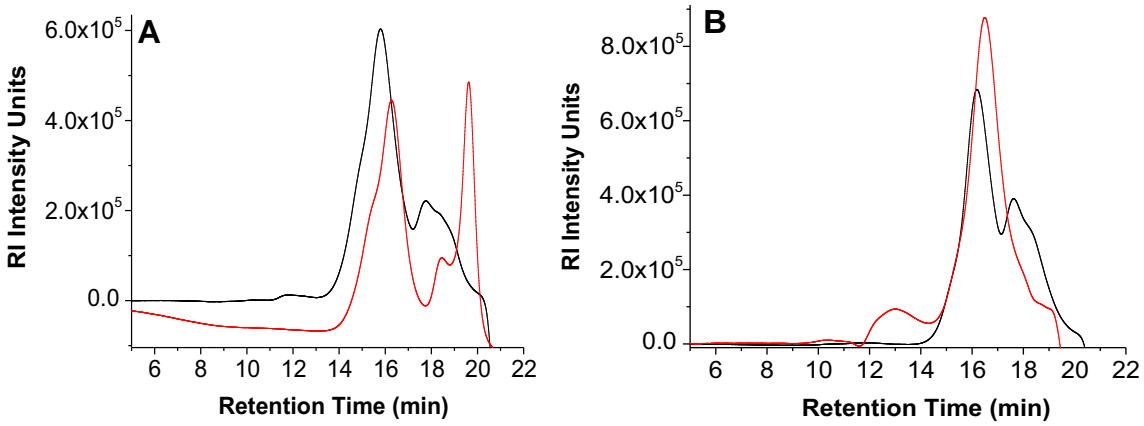

Fig. 5. Gel permeation chromatography of the (**A**) PEG_{1900}-S-S-PLA_{3600} and (**B**) PEG_{1900}-S-S-PLA_{5800} polymers before (black trace) and after (red trace) incubation with 5 mM of GSH for 60 min. (For interpretation of the references to color in this figure legend, the reader is referred to the web version of this article.)

incubation with 5 mM GSH, the spherical structures of the polymersomes were completely destroyed (Fig. 6, after treatment).

3.3. Demonstration of the polymersomes' echogenicity

We have previously established that echogenic liposomes can be prepared in the presence of at least 100 mM of mannitol as a cryoprotectant [46], and the ideal concentration is 320 mM. In this study, we used 320 mM of mannitol to prepare the echogenic polymersomes. The defects in the encapsulating layer created during the freeze–thaw and lyophilization process (mannitol is a weak cryoprotectant and cannot provide adequate protection for the bilayer) allow entrapment of air during the reconstitution of the lyophilized powder in a buffer solution [50,58]. This method allows the entrapment of air inside vesicles, enabling them to reflect ultrasound. Although the exact location of air has not been determined conclusively, there are reports of air being trapped in the hydrophobic part of shell or inside the aqueous interior [59].

To demonstrate echogenicity of the polymersomes, we studied their acoustic properties using an *in-vitro* acoustic setup (shown in Fig. 1) and diagnostic ultrasound imaging. The excitation pulse consisted of a 32-cycle sinusoidal wave with a frequency of 3.5 MHz and with an acoustic pressure amplitude of 250 kPa. A polymersome concentration of 10 μg/mL was used for all *in-vitro* acoustic experiments without any problem of signal attenuation due to the setup design. Fig. 7 shows the scattered response from the **P4** and **P5** polymersome samples. Note that, for the **P5** batch, both second-harmonic and subharmonic components were detected in the scattered acoustic spectra. Hence, all three components, i.e., fundamental, subharmonic, and second-harmonic, are shown for

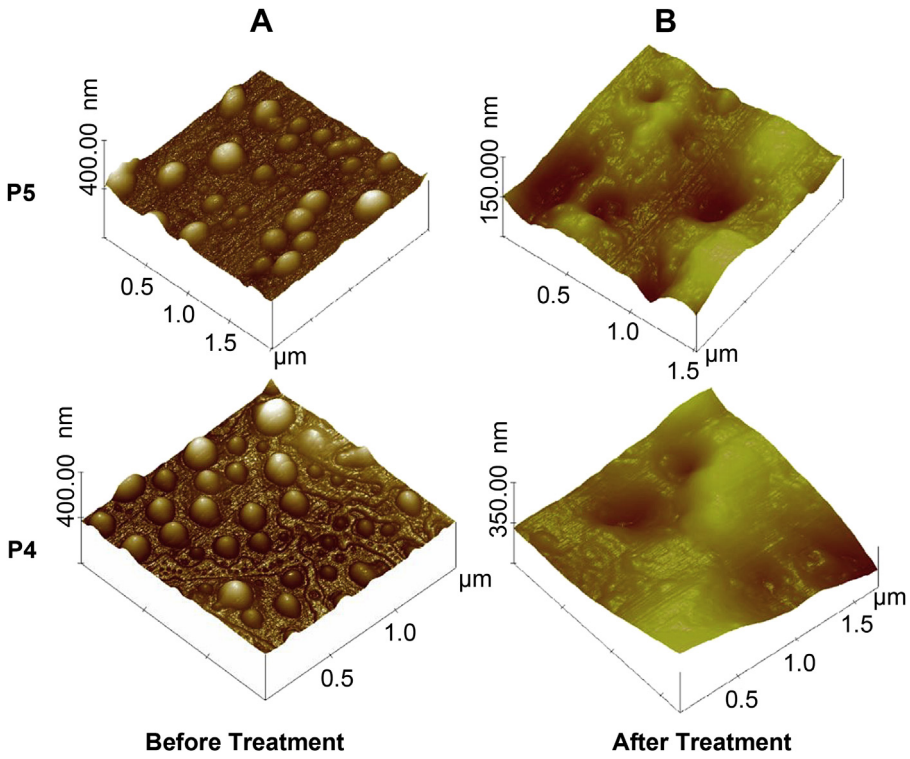

Fig. 6. Atomic force microscopic images of **P5** polymersomes and **P4** polymersomes before and after incubation with 5 mM of glutathione for 1 h.

Table 2
Physical characterization of the **P4** and **P5** polymersomes ($n = 5$).

Polymersomes	Zeta potential (mV)	Mobility (μm cm/Vs)	Size (nm)	PDI
P4	−3.2 ± 0.5	−0.25 ± 0.03	157 ± 68	0.58 ± 0.07
P5	−2.4 ± 0.6	−0.23 ± 0.04	209 ± 34	0.64 ± 0.03

comparison. Unlike the nonlinear response from microbubble-based contrast agents [60], the detection of nonlinear responses from the **P5** polymersomes was inconsistent. For the **P4** polymersomes, the nonlinear components were consistently absent in all experiments and, hence, are not shown here. The lack of a nonlinear response can either be due to the lower pressure amplitude (250 kPa) used here or due to the inherent acoustic properties of these polymersomes. Further studies are presently being conducted to verify these hypotheses.

We observed that the **P5** polymersomes show around 20 dB, 10 dB, and 4 dB enhancements over the control (i.e., without any polymersomes) for the fundamental, subharmonic, and second-harmonic components (Fig. 7). However, the enhancement was much weaker for the **P4** polymersomes; it was around 8 dB for the fundamental component. This finding indicated that modifying the copolymers' PLA block enables us to tune their acoustic properties. Because the bilayers are made of amphiphilic copolymers, we expected these polymersomes to be mechanically stable. To test this hypothesis, we performed time-dependent scattering measurements with both batches (Fig. 7C). The scattered response was stable for both batches with around 5 dB of decay over 10 min.

Echogenicity was also confirmed by imaging with a Terason t3200 ultrasonic medical imaging system using a 4–15 MHz transducer. Reconstituted polymersomes reflected the ultrasound, indicating the presence of entrapped air (Fig. 8), whereas the control samples (polymersomes before freeze drying) were devoid of such reflections. The mean and maximum gray-scale values were obtained by analyzing images with ImageJ software, and the comparison is shown in Fig. 8E and F. The echogenic **P4** and **P5** polymersomes (Fig. 8, Panels C and D) showed higher gray-scale values compared to their non-echogenic counterparts (controls; Fig. 8, Panels A and B). Moreover, the response from **P5** polymersomes was higher than the **P4** polymersomes (Fig. 8, panels C and D), further corroborating our results with the acoustic scattering experiments (Fig. 7). We also noticed that adding 5 mM of GSH to the polymersome samples reduced the ultrasound reflectivity (Supporting Information).

3.4. Demonstration of redox-triggered release from the polymersomes

After confirming the echogenicity, we checked the redox-triggered release from these polymersomes. In this endeavor, we encapsulated 10 μM of calcein dye in the **P4** and **P5** polymersomes,

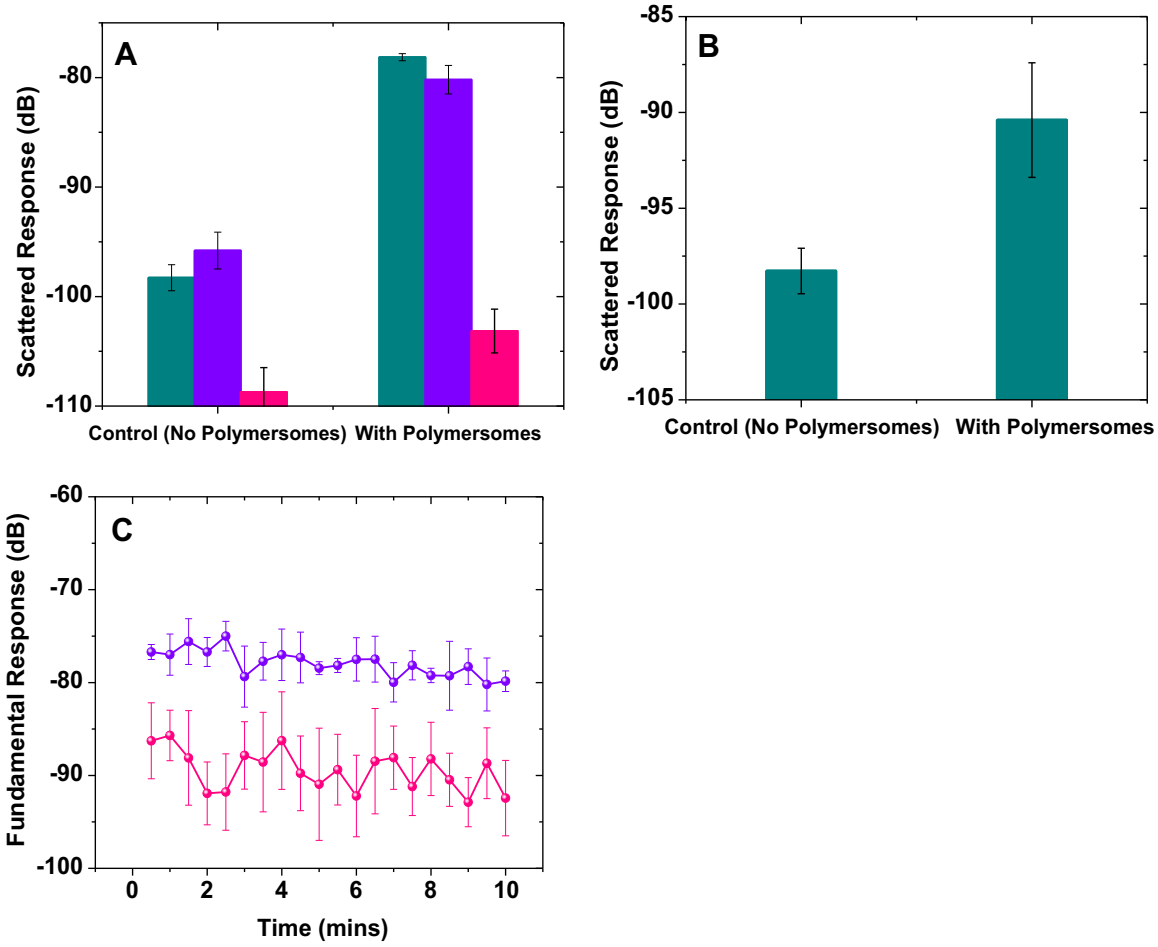

Fig. 7. Ultrasound scattered responses from echogenic polymersomes (**A**) **P5** and (**B**) **P4** (dark cyan: fundamental, violet: subharmonic, and pink: second-harmonic responses). (**C**) Time-dependent scattering responses from polymersomes **P5** (violet) and **P4** (pink) ($n = 3$). (For interpretation of the references to color in this figure legend, the reader is referred to the web version of this article.)

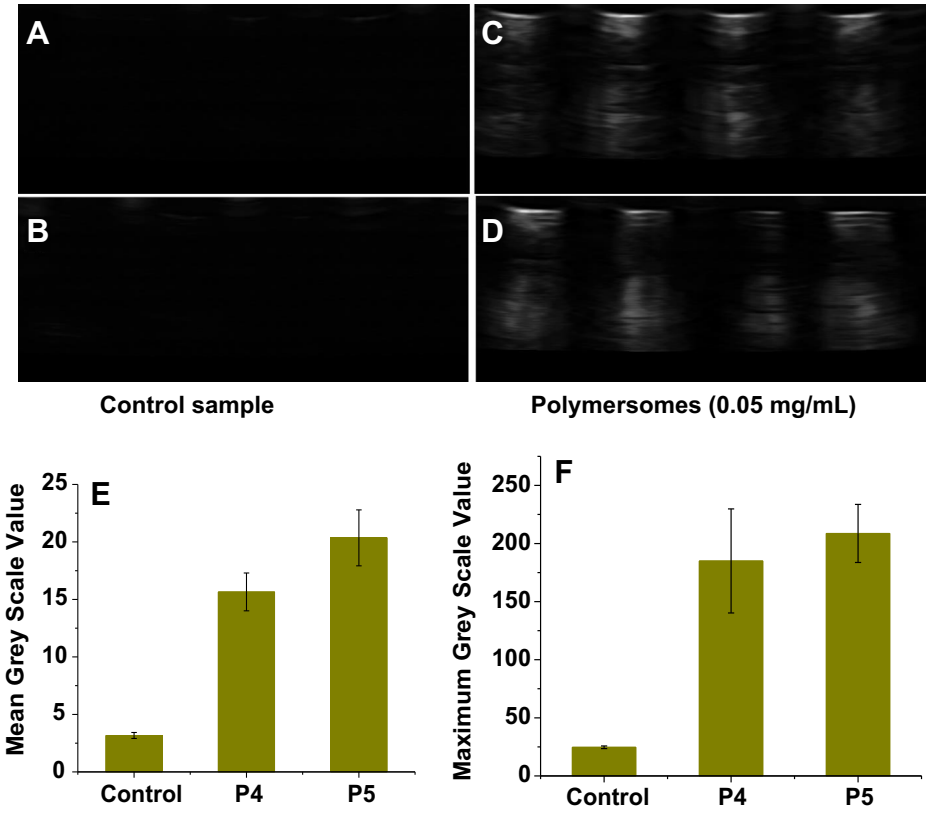

Fig. 8. Diagnostic-frequency ultrasound imaging and mean gray-scale values for the polymersomes: (**A**) **P5** polymersome before free drying (control), (**B**) **P4** polymersome before freeze drying (control), (**C**) **P5** polymersomes after freeze drying, (**D**) **P4** polymersomes after freeze drying, (**E**) mean gray-scale values, and (**F**) maximum gray-scale value ($n = 3$).

and we monitored the release by using the cobalt (II) quenching method. We studied the release profiles with 3 different reducing agents: glutathione (GSH), cysteine (CYS), and dithiothreitol (DTT) at concentrations ranging from 50 μM (extracellular concentration of thiol) to 5 mM (cytosolic concentration of thiol) [61]. Glutathione and cysteine are the primary reducing agents that maintain the redox equilibrium between the intracellular (slightly reducing) and extracellular environments within tissues (slightly oxidizing) [44]. We observed that the reducing agents rapidly released contents from the polymersomes within 10 min of incubation.

Figs. 9 and 10 show the results for the release experiments with increasing concentrations of different reducing agents. When incubated in 5 mM of GSH and DTT, both the **P4** and **P5** polymersomes showed a very rapid burst release. We observed around 80% of content release from both polymersomes when incubated with 5 mM of GSH, whereas less than 5% release was observed when incubated with 50 μM of GSH.

DTT has a very low redox potential ($E_0 = -0.332$ V at pH 7.0), and it rapidly reduces the disulfide bonds compared to glutathione ($E_0 = +0.062$ V) and cysteine ($E_0 = +0.025$ V) [62]. The release profiles of the polymersomes treated with 5 mM of cysteine can be fitted with a single exponential-rate equation (Fig. 10, black trace) with rate constants of $(39 \pm 3) \times 10^{-2}\ s^{-1}$ for **P5** polymersomes and $(20 \pm 2) \times 10^{-2}\ s^{-1}$ for **P4** polymersomes. These results indicate that the polymersomes would be stable while circulating in the blood and extracellular spaces, releasing less than 5% of their

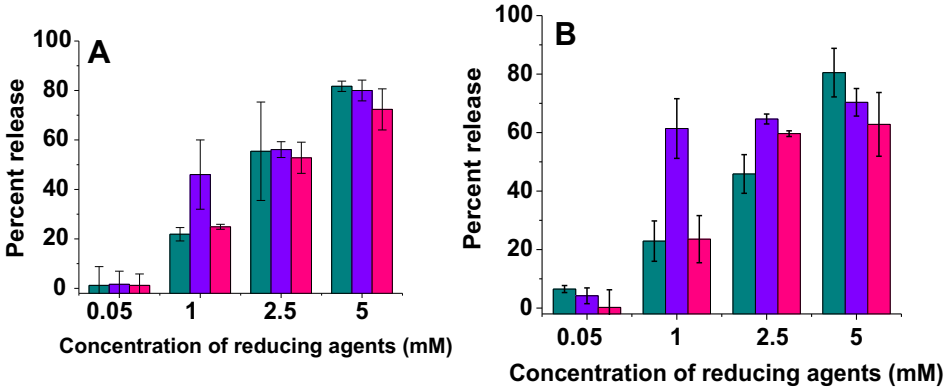

Fig. 9. Redox-triggered release as a function of the reducing agents' concentration (dark cyan: glutathione, violet: dithiothreitol, and pink: cysteine) from (**A**) polymersome **P5** and (**B**) polymersome **P4** ($n = 3$). (For interpretation of the references to color in this figure legend, the reader is referred to the web version of this article.)

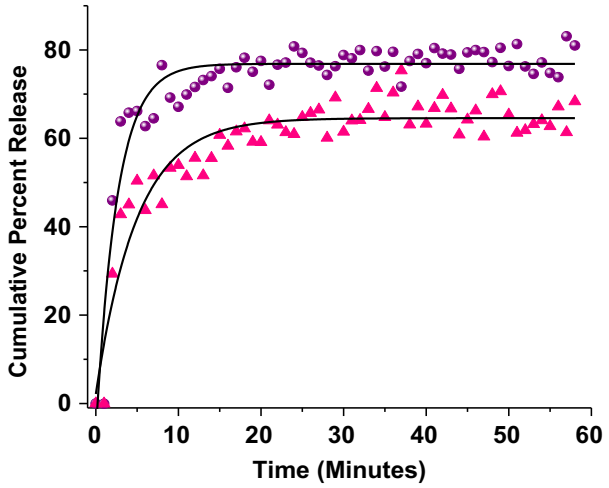

Fig. 10. Representative release profiles of calcein from polymersomes **P4** (pink triangles) and **P5** (violet spheres) when incubated with 5 mM of cysteine for an hour. The fitted curves, according to a single exponential-rate equation, are shown as black traces. (For interpretation of the references to color in this figure legend, the reader is referred to the web version of this article.)

contents. After endocytosis, they will rapidly release the encapsulated contents inside the cell cytosol.

3.5. Effect of ultrasound on the redox-triggered release from the polymersomes

Following the demonstration of reductive destabilization for the **P4** and **P5** polymersomes, we proceeded to determine their sensitivity to diagnostic-frequency ultrasound. For this purpose, we exposed the polymersomes to a 1 MHz ultrasound (continuous wave) for different time intervals, and monitored the release of the encapsulated calcein. We noted, *a priori*, that unlike liposomes, polymersomes do not exhibit high domain exchanges [63], and this may pose potential challenges for ultrasound-triggered release. We observed that both the **P4** and **P5** polymersomes failed to release the encapsulated dye in the presence of the applied ultrasound.

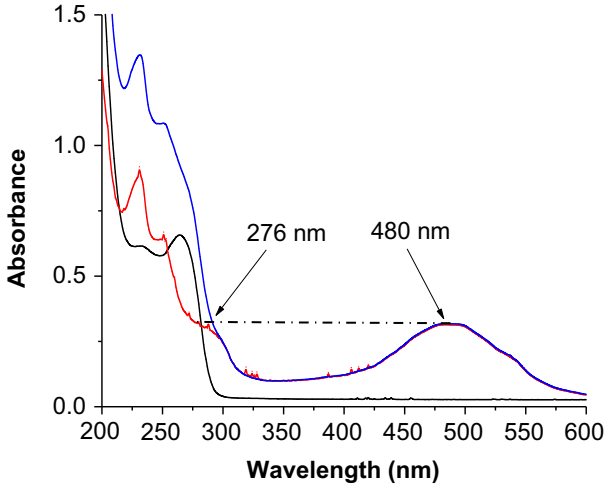

Fig. 11. Dual-wavelength UV spectrophotometric method for simultaneous determination of gemcitabine and doxorubicin. The absorption spectra for gemcitabine (black trace), doxorubicin (red trace), and the combination (blue trace) are shown. (For interpretation of the references to color in this figure legend, the reader is referred to the web version of this article.)

Table 3
Encapsulation efficiencies of gemcitabine and doxorubicin into the polymersomes using the pH gradient method ($n = 3$).

Polymersomes	Gemcitabine		Doxorubicin	
	Conc. (μg/mL)	Percent entrapment	Conc. (μg/mL)	Percent entrapment
P5	31.6 ± 6.1	41.7 ± 4.5	20.8 ± 7.4	27.2 ± 7.5
P5 folate	39.6 ± 9.8	46.1 ± 9.1	20.8 ± 5.8	27.4 ± 5.5
P4	34.7 ± 7.5	45.7 ± 6.0	20.7 ± 7.9	27.2 ± 7.0
P4 folate	29.9 ± 4.3	39.4 ± 2.2	16.9 ± 5.7	22.2 ± 5.7

Increasing the ultrasound's intensity (0.1–2 W/cm^2), duty cycles (10%–100%), and duration (1 min–15 min) of application did not have any observable effects either. We attributed these negative results to the mechanical and thermodynamic stability of the polymersomes' bilayer. By employing transmission electron microscopy, we observed the bilayers to be 20–30 nm thick (Fig. 3, Panels D and E), attesting to the mechanical stability of the polymersomes.

Subsequently, we studied the effects of simultaneously applying a reducing agent and ultrasound on the contents released from the polymersomes. Although we observed some enhancements (5–10%) in the release due to the application of ultrasound (with the reducing agents GSH and CYS), the results were inconsistent. This lack of consistency may be due to the wide size distribution of polymersomes with a polydispersity index of 0.6 (Table 2). Because the polymersomes have heterogeneous sizes, they are expected to respond to ultrasound differently; the larger-sized vesicles couple more efficiently with the ultrasound waves. In addition, the reducing agents alone release the encapsulated contents rather rapidly (Figs. 9 and 10). Because the reducing agents destroy the polymersome structures (Fig. 6), the entrapped air is likely to escape, making polymersomes less responsive to the applied ultrasound.

3.6. Simultaneous encapsulation of gemcitabine and doxorubicin in the polymersomes

Following these studies, we proceeded to simultaneously encapsulate the anticancer drugs, gemcitabine and doxorubicin, into the **P4** and **P5** polymersomes. This combination is reported to be more effective compared to the individual drugs [64]. Currently, more than 80 clinical trials are in progress (www.clinicaltrials.gov; accessed on February 28, 2014) to test the efficacy of liposomal doxorubicin (Doxil) in combination with injections of gemcitabine for the treatment of various cancers [9,18,65].

Prior to encapsulating doxorubicin and gemcitabine into the polymersomes, we developed a UV spectrophotometric, dual-wavelength method to determine their solution concentrations. Although liquid chromatographic methods are frequently-used for simultaneous determination of two or more drugs, they are expensive and time consuming [66,67]. Specifically, we selected two wavelengths so that doxorubicin has equal absorbance at both the wavelengths and that, at one of the wavelengths, gemcitabine absorbance is negligible. By comparing the absorption spectra for the two drugs (Fig. 11), we selected 480 nm and 276 nm as the wavelengths of choice. At 480 nm, doxorubicin can be determined reliably because gemcitabine absorbance is negligible at this wavelength. Because doxorubicin absorbs equally at 276 nm and 480 nm, gemcitabine can be determined at 276 nm by subtracting the absorbance of doxorubicin at 480 nm from the total absorbance at 276 nm (Fig. 11). Following this strategy, we established a standard calibration curve for both drugs (Supporting Information).

We compared the efficiencies for the passive- and active-loading methods to encapsulate gemcitabine and doxorubicin

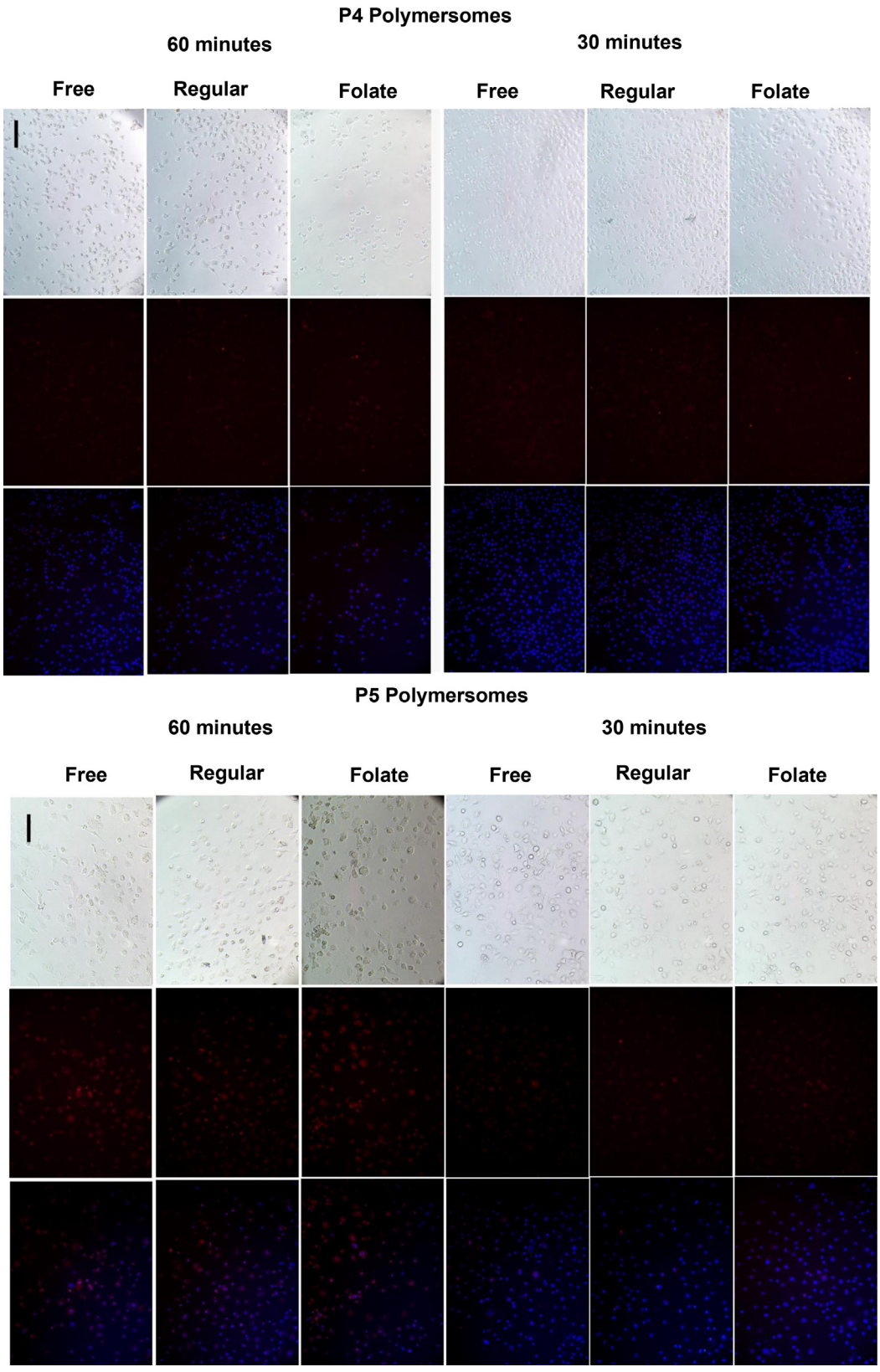

Fig. 12. Confocal fluorescence microscopic images of folate-targeted **P4** and **P5** polymersomes' uptake by PANC-1 cells as a function time (Scale bar: 100 μm).

into the polymersomes. For passive entrapment, the drugs were dissolved in a 10 mM HEPES buffer (pH = 7.4), and the solutions of the polymers in THF were added slowly. For active loading, we used the pH gradient method. We prepared the polymersomes in a citrate buffer (pH 4.0), and the external pH was neutralized by adding solid sodium bicarbonate. The polymersomes were then incubated with the drug combination. The unencapsulated drugs were separated from the polymersomes, and encapsulation

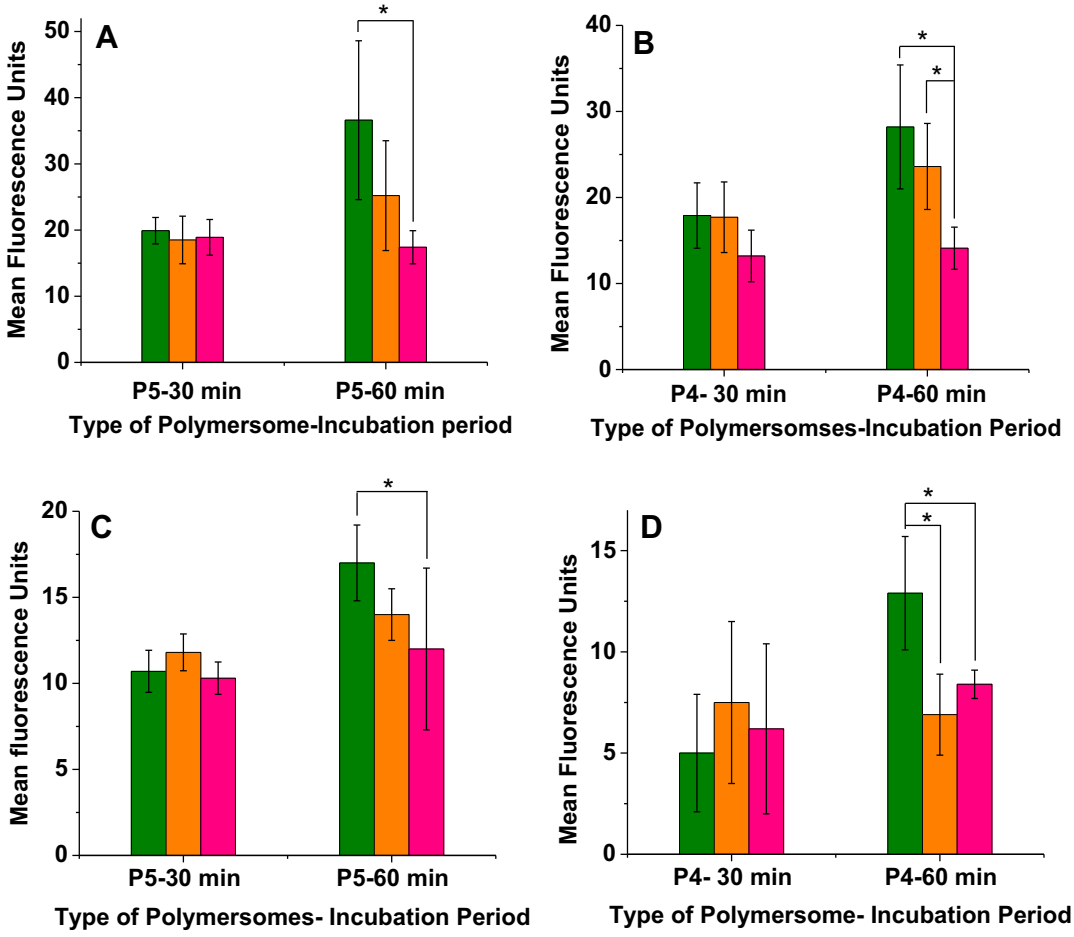

Fig. 13. Mean fluorescence analysis for the uptake of polymersomes by MCF-7 (**A** and **B**) and PANC-1 (**C** and **D**) cells. Green: folate-targeted polymersomes; orange: non-targeted, regular polymersomes; and pink: free gemcitabine and doxorubicin (*$P < 0.05$, $n = 4$). (For interpretation of the references to color in this figure legend, the reader is referred to the web version of this article.)

efficiency was established by measuring the absorbance before and after gel filtration.

The encapsulation efficiencies with the passive entrapment method were 43 ± 8% for gemcitabine and only 13 ± 4% for doxorubicin with both the **P4** and **P5** polymersomes. The pH gradient method produced a similar encapsulation efficiency for gemcitabine (43 ± 2%); however, the efficiency for doxorubicin entrapment was higher (27 ± 7%). We noticed that entrapment efficiencies were similar for both **P4** and **P5** as well as for targeted and non-targeted polymersomes (Table 3). We attributed the moderate drug entrapment to the rigidity of the polymersome bilayers, which minimizes the molecules' entry into the aqueous core. We also noted that the higher molecular weight and larger size of doxorubicin (MW: 543) led to a lower encapsulation efficiency compared to gemcitabine (MW: 263.) Heating the polymersomes above their glass transition temperature (65 °C) did not improve the encapsulation.

3.7. Demonstration of release using monolayer cell culture

Having optimized the encapsulation of the drugs, we proceeded to evaluate the active targeting of these polymersomes to cancer cells. For this endeavor, 1 mol% folate-conjugated lipid (DSPE-PEG-Folate, commercially available from NANOCS, NY) with PEG_{3400} (for **P4** polymersomes) and PEG_{5000} (for **P5** polymersomes) was added to the polymers during polymersome preparation. We selected the folate receptor overexpressing pancreatic ductal carcinoma (PANC-1) and breast cancer (MCF-7) cells for the uptake studies. After incubating the polymersomes for different times, we imaged the cells using a confocal fluorescent microscope (Fig. 12 for the PANC-1 cells; the corresponding images for the MCF-7 cells are included in the Supporting Information). We noticed that polymersomes incorporating 1 mol% of the folate lipid were taken up by cells more effectively compared to the polymersomes without the folate lipid or the free drugs. The MCF-7 cells showed faster and higher uptake of the folate-targeted polymersomes compared to PANC-1 cells. Analyses of the mean red fluorescence intensities for all images indicated that there was no significant uptake difference for the initial 30 min (Fig. 13). However, as the incubation period increased to 60 min, we observed enhanced cellular uptake for the folate-targeted polymersomes compared to the non-targeted counterparts and free drugs (Figs. 12–14).

After demonstrating successful uptake for folate-targeted polymersomes, we assessed their ability to kill these folate-receptor overexpressing cancer cells. We exposed the MCF-7 and PANC-1 cells to different treatments for various time intervals, and we analyzed cell viability by employing the AlamarBlue® assay [68]. Both the **P4** and **P5** polymersomes showed significantly higher killing of MCF-7 cells compared to the free gemcitabine + doxorubicin combination (Fig. 14A). Even non-targeted **P5** polymersomes showed significant toxicity enhancement toward MCF-7 cells compared to the free drugs

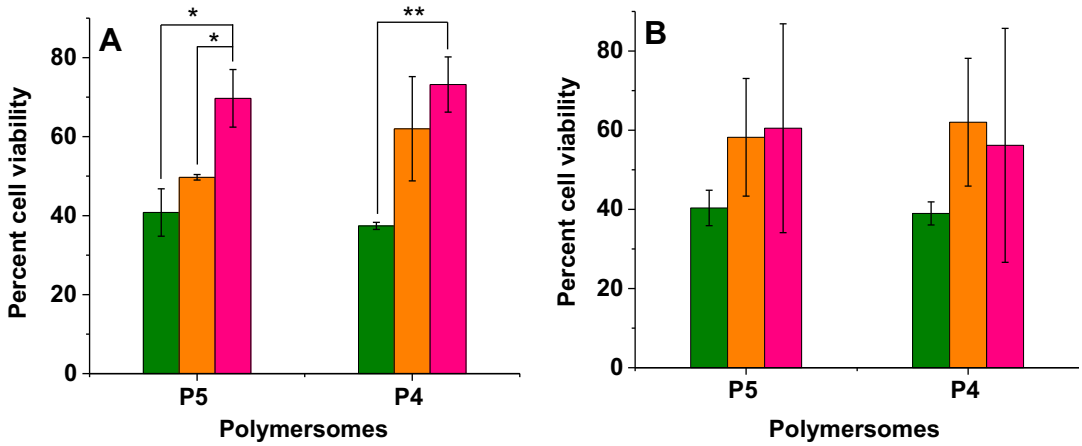

Fig. 14. Cell viability with folate-overexpressing MCF-7 cells (**A**) and PANC-1 cells (**B**) after 48-h incubation. Green: folate-targeted polymersomes, orange: non-targeted polymersomes, and pink: free gemcitabine and doxorubicin (*$P < 0.05$, **$P < 0.01$, $n = 5$). (For interpretation of the references to color in this figure legend, the reader is referred to the web version of this article.)

together. We also tested these polymersomes with the PANC-1 cell line, and we noticed that, although there was significant killing (around 60%) with folate-targeted polymersomes, it was not significantly better than non-targeted polymersomes and free drugs (Fig. 14B). These observations supported our results with uptake experiments where a significant uptake enhancement for folate-targeted polymersomes was observed in MCF-7 cells compared to the PANC-1 cells.

3.8. Demonstration of release using three-dimensional, spheroid cell culture

Although studies with a monolayer cell culture are fast, cost effective, and demonstrate a proof of concept, they also have limitations. For example, a monolayer cell culture bears little resemblance to the complex, three-dimensional growth of tumors *in vivo*. Multicellular tumor spheroids (3D cell culture) are models of intermediate complexity between the monolayer culture and tumors *in vivo* [69]. Among the various reported procedures to prepare the 3D spheroids, the liquid overlay method is widely used and convenient [54]. Following this protocol, we embedded the MCF-7 cells onto agar and added the growth media. Subsequently, the spheroids were prepared in 24-well plates by centrifuging to aggregate the cells at the center (Fig. 15A). The plates were placed in an incubator, undisturbed, and we measured the spheroid area after 3 days. When observed under a light microscope, the growing cell spheroids showed three distinct regions, similar to *in vivo* tumors (Fig. 15B). The center of the spheroid was necrotic; the cells died due to the limited availability of oxygen and nutrition (region 1). This center was surrounded by a region of inactive, but live, cells (region B2). The actively proliferating cells were at the periphery of the spheroids (region 3), which had direct access to the media (region 4). This morphology of 3D spheroids makes them a better tool for conducting *in-vitro* cellular experiments. Spheroids varied in size from 1 mm to 2 mm with distinct areas as explained earlier.

On 10th and 11th day after preparation, we exposed the MCF-7-cell spheroids to different treatments for 48 h (Fig. 16A). Areas of spheroids were monitored for each treatment group, normalized and plotted as a function of time (Fig. 16B and C). We observed that folate-targeted **P5** polymersomes were most effective among all the treatments, eliciting a significant reduction in size for the spheroids (Fig. 16B) compared to the non-targeted polymersomes and the free drugs. While the control spheroids grew by 185% of their initial size, average growth was restricted to only 73% in the presence of the folate-targeted **P5** polymersomes. We also noticed that non-targeted polymersomes did not show any improvement over the free-drug treatment. This implies that the folate targeting improved the uptake of polymersomes not only in the monolayer, but also in the three-dimensional spheroid cell culture. To our surprise, the folate-targeted **P4** polymersomes did not show any additional advantage over non-targeted polymersomes and the

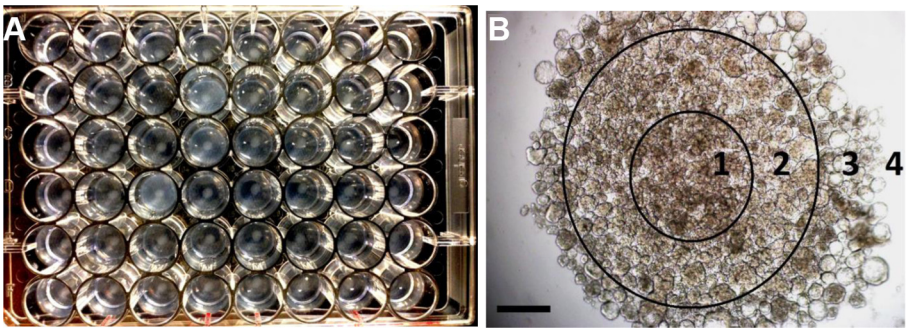

Fig. 15. Spheroid culture of MCF-7 cells: (**A**) 24-well plate coated with agar; cell aggregation was facilitated by centrifugation. (**B**) A cell spheroid showing three distinct regions, which mimic the *in vivo* conditions. Region **1**: central necrotic area (hypoxic) which gets a lesser amount of nutrition and oxygen; Region **2**: inactive/resting cells which grow slowly; Region **3**: active/proliferating cells which grow rapidly; and Region **4**: nutrition/media (scale bar at the bottom: 400 μm).

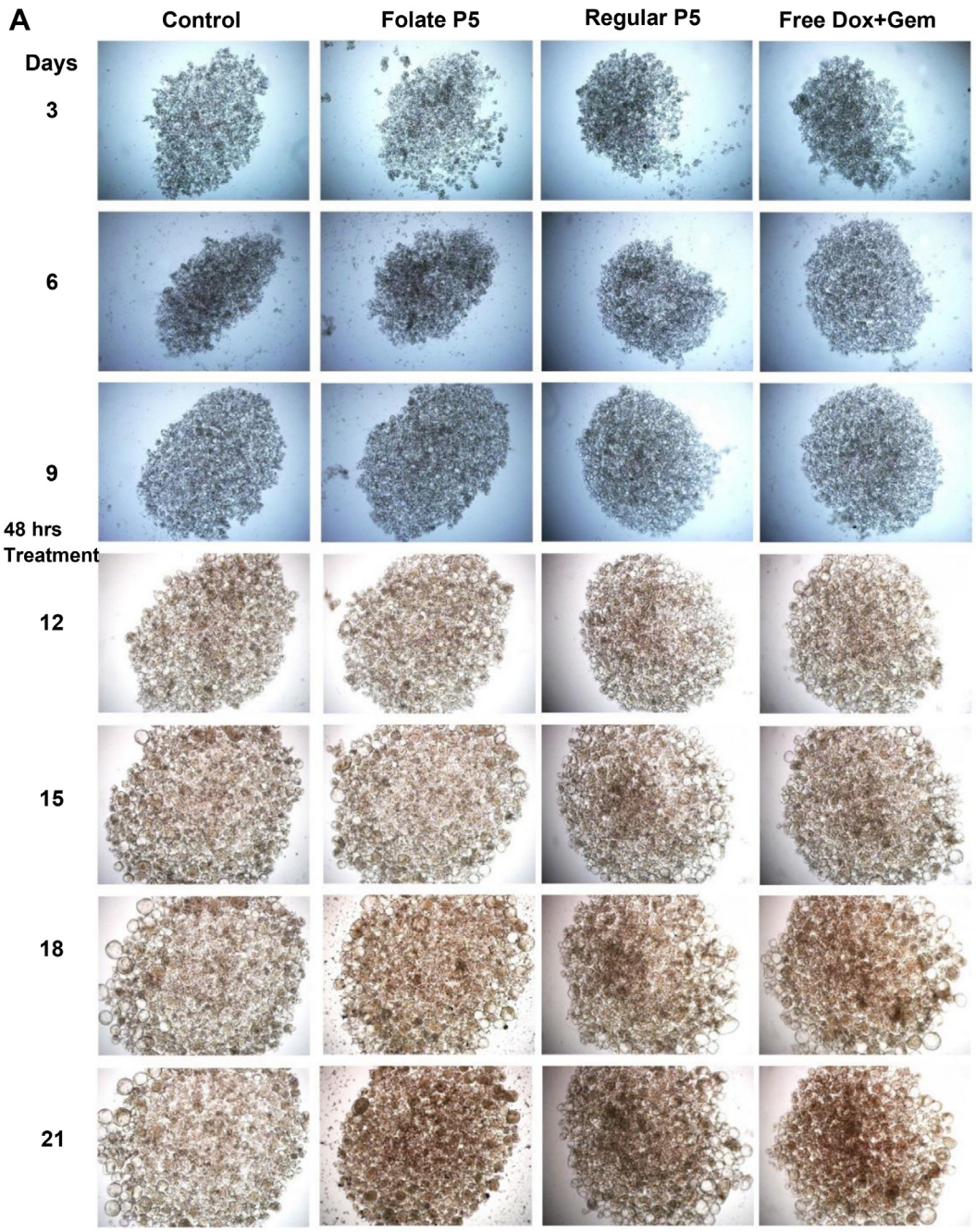

Fig. 16. (**A**) Images of MCF-7 cellular spheroids treated with **P5** polymersomes. Spheroids were exposed to three different treatments for 48 h on the 10th and 11th days. (**B**) Growth curves for the spheroids treated with **P5** polymersomes. (**C**) Growth curves for spheroids treated with **P4** polymersomes. Green stars: folate-targeted polymersomes, orange rectangles: non-targeted polymersomes, pink triangles: free gemcitabine and doxorubicin, and black spheres: control samples. ($^*P < 0.05$, $n = 5$). (For interpretation of the references to color in this figure legend, the reader is referred to the web version of this article.)

free-drug combination (Supporting Information). We do not have an explanation for this observation.

4. Conclusions

We have successfully prepared echogenic, redox-sensitive, targeted polymersomes. Ultrasound-scattering and imaging experiments confirmed the echogenicity of the vesicles. These polymersomes showed excellent release profiles when incubated with cytosolic concentrations of reducing agents, releasing more than 80% of the contents within 20 min. However, in serum levels of reducing agents, minimal release was observed. When a folate lipid was incorporated in the bilayer, the polymersomes showed an enhanced uptake with folate-receptor overexpressing breast- and pancreatic-cancer cells. A combination of the two anticancer drugs, gemcitabine and doxorubicin, was successfully encapsulated in the polymersomes. These targeted, dual-drug encapsulating polymersomes significantly decreased the viability of breast- and pancreatic-cancer cells in the monolayer as well as in spheroid cultures. Our results are expected to encourage further research about the use of ultrasound-reflective polymersomes as multimodal drug carriers with targeting and triggered release properties.

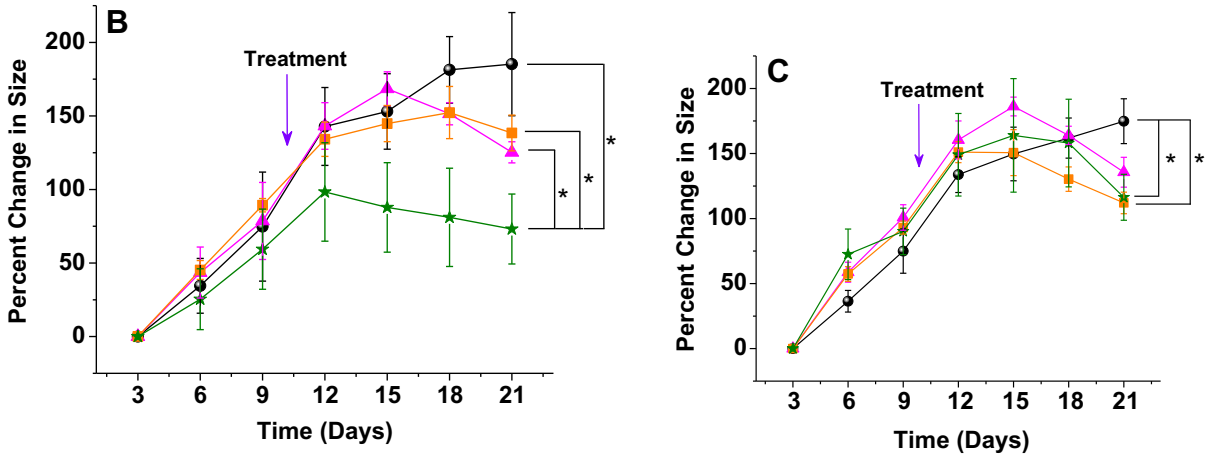

Fig. 16. (*continued*).

Acknowledgments

This research was supported by NIH grant 1R01 CA 113746 as well as NSF grants DMR 1005011 and DMR 1306154 to SM; DMR 1005283, and NIH grant P20RR016472 to KS.

Appendix A. Supplementary data

Supplementary data related to this article can be found at http://dx.doi.org/10.1016/j.biomaterials.2014.04.026.

References

[1] Toschi L, Finocchiaro G, Bartolini S, Gioia V, Cappuzzo F. Role of gemcitabine in cancer therapy. Future Oncol 2005;1:7–17.
[2] Dasanu CA. Gemcitabine: vascular toxicity and prothrombotic potential. Expert Opin Drug Saf 2008;7:703–16.
[3] Moog R, Burger AM, Brandl M, Schuler J, Schubert R, Unger C, et al. Change in pharmacokinetic and pharmacodynamic behavior of gemcitabine in human tumor xenografts upon entrapment in vesicular phospholipid gels. Cancer Chemother Pharmacol 2002;49:356–66.
[4] Farrell JJ, Elsaleh H, Garcia M, Lai R, Ammar A, Regine WF, et al. Human equilibrative nucleoside transporter 1 levels predict response to gemcitabine in patients with pancreatic cancer. Gastroenterology 2009;136:187–95.
[5] Lee GY, Qian WP, Wang L, Wang YA, Staley CA, Satpathy M, et al. Theranostic nanoparticles with controlled release of gemcitabine for targeted therapy and MRI of pancreatic cancer. ACS Nano 2013;7:2078–89.
[6] Dalla Pozza E, Lerda C, Costanzo C, Donadelli M, Dando I, Zoratti E, et al. Targeting gemcitabine containing liposomes to CD44 expressing pancreatic adenocarcinoma cells causes an increase in the antitumoral activity. Biochim Biophys Acta 2013;1828:1396–404.
[7] Zhu S, Wonganan P, Lansakara PD, O'Mary HL, Li Y, Cui Z. The effect of the acid-sensitivity of 4-(N)-stearoyl gemcitabine-loaded micelles on drug resistance caused by RRM1 overexpression. Biomaterials 2013;34:2327–39.
[8] Kotopoulis S, Dimcevski G, Gilja OH, Hoem D, Postema M. Treatment of human pancreatic cancer using combined ultrasound, microbubbles, and gemcitabine: a clinical case study. Med Phys 2013;40:072902.
[9] Julka PK, Chacko RT, Nag S, Parshad R, Nair A, Koppiker CB, et al. A phase 2 study of sequential neoadjuvant chemotherapy with gemcitabine and doxorubicin followed by gemcitabine and cisplatin in patients with large or locally advanced operable breast cancer: results from long-term follow-up. Breast Cancer 2013;20:357–62.
[10] Crespo G, Sierra M, Losa R, Berros JP, Villanueva N, Fra J, et al. Pegylated liposomal doxorubicin and gemcitabine in a fixed dose rate infusion for the treatment of patients with poor prognosis of recurrent ovarian cancer: a phase Ib study. Int J Gynecol Cancer 2011;21:478–85.
[11] Del Barco S, Colomer R, Calvo L, Tusquets I, Adrover E, Sanchez P, et al. Non-pegylated liposomal doxorubicin combined with gemcitabine as first-line treatment for metastatic or locally advanced breast cancer. Final results of a phase I/II trial. Breast Cancer Res Treat 2009;116:351–8.
[12] Roubaud G, Gross-Goupil M, Wallerand H, de Clermont H, Dilhuydy MS, Ravaud A. Combination of gemcitabine and doxorubicin in rapidly progressive metastatic renal cell carcinoma and/or sarcomatoid renal cell carcinoma. Oncology 2011;80:214–8.
[13] Franchina T, Adamo B, Ricciardi GR, Caristi N, Agostino RM, Proto C, et al. Activity of pegylated liposomal doxorubicin in combination with gemcitabine in triple negative breast cancer with skin involvement: two case reports. Cancer Biol Ther 2012;13:472–6.
[14] Rivera E, Valero V, Arun B, Royce M, Adinin R, Hoelzer K, et al. Phase II study of pegylated liposomal doxorubicin in combination with gemcitabine in patients with metastatic breast cancer. J Clin Oncol 2003;21:3249–54.
[15] Fabi A, Ferretti G, Papaldo P, Salesi N, Ciccarese M, Lorusso V, et al. Pegylated liposomal doxorubicin in combination with gemcitabine: a phase II study in anthracycline-naive and anthracycline pretreated metastatic breast cancer patients. Cancer Chemother Pharmacol 2006;57:615–23.
[16] Liu D, Chen Y, Feng X, Deng M, Xie G, Wang J, et al. Micellar nanoparticles loaded with gemcitabine and doxorubicin showed synergistic effect. Colloids Surf B Biointerfaces 2013;113C:158–68.
[17] Rivera E, Valero V, Syrewicz L, Rahman Z, Esteva FJ, Theriault RL, et al. Phase I study of stealth liposomal doxorubicin in combination with gemcitabine in the treatment of patients with metastatic breast cancer. J Clin Oncol 2001;19:1716–22.
[18] D'Agostino G, Ferrandina G, Ludovisi M, Testa A, Lorusso D, Gbaguidi N, et al. Phase II study of liposomal doxorubicin and gemcitabine in the salvage treatment of ovarian cancer. Br J Cancer 2003;89:1180–4.
[19] Jacquin JP, Chargari C, Thorin J, Mille D, Melis A, Orfeuvre H, et al. Phase II trial of pegylated liposomal doxorubicin in combination with gemcitabine in metastatic breast cancer patients. Am J Clin Oncol 2012;35:18–21.
[20] Lammers T, Subr V, Ulbrich K, Peschke P, Huber PE, Hennink WE, et al. Simultaneous delivery of doxorubicin and gemcitabine to tumors in vivo using prototypic polymeric drug carriers. Biomaterials 2009;30:3466–75.
[21] Barenholz Y. Doxil(R)–the first FDA-approved nano-drug: lessons learned. J Control Release 2012;160:117–34.
[22] Maeda H, Matsumura Y. EPR effect based drug design and clinical outlook for enhanced cancer chemotherapy. Adv Drug Deliv Rev 2011;63:129–30.
[23] Discher DE, Ortiz V, Srinivas G, Klein ML, Kim Y, Christian D, et al. Emerging applications of polymersomes in delivery: from molecular dynamics to shrinkage of tumors. Prog Polym Sci 2007;32:838–57.
[24] Szebeni J, Baranyi L, Savay S, Bodo M, Morse DS, Basta M, et al. Liposome-induced pulmonary hypertension: properties and mechanism of a complement-mediated pseudoallergic reaction. Am J Physiol Heart Circ Physiol 2000;279:H1319–28.
[25] Nahire R, Haldar MK, Paul S, Mergoum A, Ambre AH, Katti KS, et al. Polymer-coated echogenic lipid nanoparticles with dual release triggers. Biomacromolecules 2013;14:841–53.
[26] Nahire R, Paul S, Scott MD, Singh RK, Muhonen WW, Shabb J, et al. Ultrasound enhanced matrix metalloproteinase-9 triggered release of contents from echogenic liposomes. Mol Pharm 2012;9:2554–64.
[27] Lee JS, Feijen J. Polymersomes for drug delivery: design, formation and characterization. J Control Release 2012;161:473–83.
[28] Meng F, Zhong Z, Feijen J. Stimuli-responsive polymersomes for programmed drug delivery. Biomacromolecules 2009;10:197–209.
[29] Jain JP, Ayen WY, Kumar N. Self assembling polymers as polymersomes for drug delivery. Curr Pharm Des 2011;17:65–79.
[30] Choucair A, Soo PL, Eisenberg A. Active loading and tunable release of doxorubicin from block copolymer vesicles. Langmuir 2005;21:9308–13.
[31] Ahmed F, Discher DE. Self-porating polymersomes of PEG-PLA and PEG-PCL: hydrolysis-triggered controlled release vesicles. J Control Release 2004;96:37–53.
[32] Chiang WH, Huang WC, Chang CW, Shen MY, Shih ZF, Huang YF, et al. Functionalized polymersomes with outlayered polyelectrolyte gels for potential tumor-targeted delivery of multimodal therapies and MR imaging. J Control Release 2013;168:280–8.

[33] Canton I, Battaglia G. Polymersomes-mediated delivery of fluorescent probes for targeted and long-term imaging in live cell microscopy. Methods Mol Biol 2013;991:343–51.
[34] Petersen MA, Hillmyer MA, Kokkoli E. Bioresorbable polymersomes for targeted delivery of Cisplatin. Bioconjug Chem 2013;24:533–43.
[35] Zhang Y, Zhang W, Johnston AH, Newman TA, Pyykko I, Zou J. Targeted delivery of Tet1 peptide functionalized polymersomes to the rat cochlear nerve. Int J Nanomedicine 2012;7:1015–22.
[36] Zhou W, Meng F, Engbers GH, Feijen J. Biodegradable polymersomes for targeted ultrasound imaging. J Control Release 2006;116:e62–4.
[37] Ahmed F, Pakunlu RI, Srinivas G, Brannan A, Bates F, Klein ML, et al. Shrinkage of a rapidly growing tumor by drug-loaded polymersomes: pH-triggered release through copolymer degradation. Mol Pharm 2006;3:340–50.
[38] Gaitzsch J, Canton I, Appelhans D, Battaglia G, Voit B. Cellular interactions with photo-cross-linked and pH-sensitive polymersomes: biocompatibility and uptake studies. Biomacromolecules 2012;13:4188–95.
[39] Kim H, Kang YJ, Kang S, Kim KT. Monosaccharide-responsive release of insulin from polymersomes of polyboroxole block copolymers at neutral pH. J Am Chem Soc 2012;134:4030–3.
[40] Cerritelli S, Velluto D, Hubbell JA. PEG-SS-PPS: reduction-sensitive disulfide block copolymer vesicles for intracellular drug delivery. Biomacromolecules 2007;8:1966–72.
[41] Kamat NP, Robbins GP, Rawson JS, Therien MJ, Dmochowski IJ, Hammer DA. A generalized system for photo-responsive membrane rupture in polymersomes. Adv Funct Mater 2010;20:2588–96.
[42] Amstad E, Kim SH, Weitz DA. Photo- and thermoresponsive polymersomes for triggered release. Angew Chem Int Ed Engl 2012;51:12499–503.
[43] Oliveira H, Perez-Andres E, Thevenot J, Sandre O, Berra E, Lecommandoux S. Magnetic field triggered drug release from polymersomes for cancer therapeutics. J Control Release 2013;169:165–70.
[44] Saito G, Swanson JA, Lee KD. Drug delivery strategy utilizing conjugation via reversible disulfide linkages: role and site of cellular reducing activities. Adv Drug Deliv Rev 2003;55:199–215.
[45] West KR, Otto S. Reversible covalent chemistry in drug delivery. Curr Drug Discov Technol 2005;2:123–60.
[46] Paul S, Russakow D, Nahire R, Nandy T, Ambre AH, Katti K, et al. In vitro measurement of attenuation and nonlinear scattering from echogenic liposomes. Ultrasonics 2012;52:962–9.
[47] Robert JL, Aubrecht KB. Ring-opening polymerization of lactide to form a biodegradable polymer. J Chem Educ 2008;85:258.
[48] Mayer LD, Tai LC, Bally MB, Mitilenes GN, Ginsberg RS, Cullis PR. Characterization of liposomal systems containing doxorubicin entrapped in response to pH gradients. Biochim Biophys Acta 1990;1025:143–51.
[49] Nahire RR, Joshi SS, Meghnani V, Shastri N, Surendra Nath KV, Sathish J. Zero absorbance UV spectrophotometric assay method for simultaneous determination of amlodipine besylate and valsartan. Curr Res Bio Pharm Sci 2013;2:1–5.
[50] Kopechek JA, Abruzzo TM, Wang B, Chrzanowski SM, Smith DA, Kee PH, et al. Ultrasound-mediated release of hydrophilic and lipophilic agents from echogenic liposomes. J Ultrasound Med 2008;27:1597–606.
[51] Kopechek JA, Kim H, McPherson DD, Holland CK. Calibration of the 1-MHz Sonitron ultrasound system. Ultrasound Med Biol 2010;36:1762–6.
[52] Hensel K, Mienkina MP, Schmitz G. Analysis of ultrasound fields in cell culture wells for in vitro ultrasound therapy experiments. Ultrasound Med Biol 2011;37:2105–15.
[53] Albrecht T, Patel N, Cosgrove DO, Jayaram V, Blomley MJ, Eckersley R. Enhancement of power Doppler signals from breast lesions with the ultrasound contrast agent EchoGen emulsion: subjective and quantitative assessment. Acad Radiol 1998;5(Suppl 1):S195–8. discussion S9.
[54] Ho WY, Yeap SK, Ho CL, Rahim RA, Alitheen NB. Development of multicellular tumor spheroid (MCTS) culture from breast cancer cell and a high throughput screening method using the MTT assay. PLoS One 2012;7:e44640.
[55] Jeong B, Bae YH, Lee DS, Kim SW. Biodegradable block copolymers as injectable drug-delivery systems. Nature 1997;388:860–2.
[56] Discher DE, Ahmed F. Polymersomes. Annu Rev Biomed Eng 2006;8:323–41.
[57] Liu D, Mori A, Huang L. Role of liposome size and RES blockade in controlling biodistribution and tumor uptake of GM1-containing liposomes. Biochim Biophys Acta 1992;1104:95–101.
[58] Alkan-Onyuksel H, Demos SM, Lanza GM, Vonesh MJ, Klegerman ME, Kane BJ, et al. Development of inherently echogenic liposomes as an ultrasonic contrast agent. J Pharm Sci 1996;85:486–90.
[59] Paul S, Nahire R, Mallik S, Sarkar K. Encapsulated microbubbles and echogenic liposomes for contrast ultrasound imaging and targeted drug delivery. Comput Mech 2014;53:413–35.
[60] Jimenez-Fernandez J. Nonlinear response to ultrasound of encapsulated microbubbles. Ultrasonics 2012;52:784–93.
[61] Cleland WW. Dithiothreitol, a new protective reagent for Sh groups. Biochemistry 1964;3:480–2.
[62] Green DE. The reduction potentials of cysteine, glutathione and glycylcysteine. Biochem J 1933;27:678–89.
[63] Spinler K, Tian A, Christian DA, Pantano DA, Baumgart T, Discher DE. Dynamic domains in polymersomes: mixtures of polyanionic and neutral diblocks respond more rapidly to changes in calcium than to pH. Langmuir 2013;29:7499–508.
[64] Perez-Manga G, Lluch A, Alba E, Moreno-Nogueira JA, Palomero M, Garcia-Conde J, et al. Gemcitabine in combination with doxorubicin in advanced breast cancer: final results of a phase II pharmacokinetic trial. J Clin Oncol 2000;18:2545–52.
[65] Lombardi G, Zustovich F, Farinati F, Cillo U, Vitale A, Zanus G, et al. Pegylated liposomal doxorubicin and gemcitabine in patients with advanced hepatocellular carcinoma: results of a phase 2 study. Cancer 2011;117:125–33.
[66] Nahire RR, Joshi SS, Meghnani V, Shastri N, Nath KS, Sathish J. Stability indicating RP-HPLC method for simultaneous determination of amlodipine besylate and valsartan combination in bulk and commercial dosage forms. Asian J Pharm Life Sci 2012;2:280–90.
[67] Joshi SS, Nahire RR, Shastri N, Surendranath KV, Satish J. Validated stability-indicating RP-HPLC UV method for simultaneous determination of metformin and repaglinide. Acta Chromatogr 2012;24:419–32.
[68] Hamid R, Rotshteyn Y, Rabadi L, Parikh R, Bullock P. Comparison of alamar blue and MTT assays for high through-put screening. Toxicol Vitro 2004;18:703–10.
[69] Goodman TT, Ng CP, Pun SH. 3-D tissue culture systems for the evaluation and optimization of nanoparticle-based drug carriers. Bioconjug Chem 2008;19:1951–9.